Laser-Induced Fluorescence for Ion Tomography in a Penning Trap

Bryan A. Vining, Guo-Zhong Li,* and Alan G. Marshall
Center for Interdisciplinary Magnetic Resonance, National High Magnetic Field Laboratory, Florida State University, Tallahassee, Florida, USA

Laser-induced ion fluorescence of laser-desorbed Ba^+ ions provides a measure of the relative number of ions near the center of the Penning trap of a Fourier transform ion cyclotron resonance mass spectrometer. Here, we report the detection of Penning-trapped ions by ion fluorescence, subject to radially outward ion cloud expansion (because of ion–neutral collisions), radially inward ion cloud compression (because of quadrupolar axialization), and the effects of buffer gas pressure and electrostatic trapping potential on those processes. At high pressure and high trapping voltage, radial ejection is far more rapid than axial ejection; quadrupolar axialization increases the number of ions near the center of the trap as well as the length of time that ions may be trapped; higher pressure results in faster magnetron radial expansion; and the choice of azimuthal quadrupolar excitation waveform significantly affects the efficacy of axialization. Based on these results, we suggest that directly detected laser-induced ion fluorescence provides a general new tool for mapping the ion distribution and its time evolution in response to various excitatory and damping effects. (J Am Soc Mass Spectrom 1998, 9, 925–930) © 1998 American Society for Mass Spectrometry

The ion spatial distribution and its time evolution in a Fourier transform-ion cyclotron resonance (FT-ICR) mass spectrometer at each stage of an experiment are critical in evaluating theoretical models and for optimizing performance. The total number of trapped ions may be estimated by pulsing the ions axially to an electrometer connected to one of the end cap electrodes [1]; however, that approach does not reveal the spatial distribution of the ions. The most common method for determining the number of trapped ions has been to detect ion image current induced on opposed detector electrodes [2, 3]; however, that method detects only spatially coherent ions (i.e., ions that are spatially localized and moving together). Alternatively, ions near the axial symmetry axis in one compartment of a dual Penning trap may be located according to whether or not they can be transferred to the other compartment of the trap and dipole excited/detected there [4]. Finally, Guan et al. analyzed the time dependence of $W(CO_6^+$ ion magnetron radial diffusion to determine the ion initial magnetron radial distribution [5].

A different way to determine the ion spatial distribution is to detect ions excited by a narrow laser beam, thereby detecting only those ions in the path of that beam as it traverses the ion trap. Laser-induced fluorescence (LIF) of atomic ions confined in a Penning trap was first observed in 1980 by Drullinger et al. [6], who examined laser cooling of Mg^+ ions by LIF. Thompson et al. [7] have also investigated LIF of atomic Mg^+ ions confined in a Penning trap. In 1985 Bollinger et al. [8] detected optical–optical double resonance of Be^+ ions in a Penning trap. Itano et al. reported microwave-optical double-resonance measurements of Hg^+ ions that same year [9]. Earlier in this decade, Werth's group detected LIF [10] and optical-microwave double resonance [11] of Ba^+ ions confined in a 6-tesla Penning trap.

Alternatively, various researchers have examined LIF of atomic ions confined in a Paul trap [12–15]. Mahan et al. [16] studied the LIF of N_2^+ ions confined in a Paul trap in 1982. Kato et al. [17] observed LIF of N_2^+ ions by selected ion flow tube techniques. Welling et al. this year observed a 3-GHz difference in fluorescence excitation frequency for $^{24}Mg^+$ and $^{25}Mg^+$ [18].

Recently, Hemberger et al. [19] introduced laser photodissociation as a basis for ion tomography in a Paul trap; ions photodissociated by the laser were subsequently detected by observing product ions from that process. In a Paul trap, laser photodissociation ion tomography has been used to measure the position, velocity, and kinetic energy of resonantly excited ions [20], as well as the radial distribution and mass-selective ejection of molecular ions [21]. The Werth group took the idea a step farther, by direct detection of LIF from Ca^+ ions in a Paul trap, and used it to map the stability diagram at unprecedentedly high resolution, to

Address reprint requests to Alan G. Marshall, Department of Chemistry, Florida State University, Tallahassee, FL 32310. E-mail: marshall@magnet.fsu.edu

* Present address: Instrument Core Technology, Waters Corporation, 34 Maple Street, Milford, MA 01757-3696.

1044-0305/98/$19.00
PII S1044-0305(98)00062-2

Received February 4, 1998
Revised April 21, 1998
Accepted April 21, 1998

reveal several families of instabilities related to combinations of ion eigenfrequencies [22]. The great advantage of fluorescence detection is that the signal originates directly from the excited ion at the spatial position struck by the laser beam, rather than indirectly (as in photodissociation) from fragmentation and electrical detection of fragment ions after multiple oscillations in the trap.

Recently, we successfully detected LIF from trapped, mass-selected Ba^+ ions in the Penning trap of an FT-ICR mass spectrometer [23]. Here, we detect LIF as a measure of the relative number of atomic Ba^+ ions intercepted within the cross section of a laser beam directed axially along the magnetic field symmetry axis. Specifically, we are then able to examine the time evolution of ions during radially outward magnetron radius expansion [5], radially inward magnetron radius compression by quadrupolar axialization [24–26], and the effects of buffer gas pressure and electrostatic trapping potential on those processes.

Experimental

All of the experiments detailed in this article were performed with a 3-tesla FT-ICR instrument described previously [23]. We obtained fluorescence from Ba^+ ions by laser desorption of solid barium at 1064 nm by use of a Nd:YAG, Q-switched laser. A tunable dye laser, pumped by the Nd:YAG laser, provided the excitation energy for fluorescence. The laser beam used to induce fluorescence passes along the symmetry axis of an open three-section cylindrical Penning trap. Thus, the measured fluorescence is a measure of the number of ions intercepted by a laser beam of ~2 mm diameter directed along the symmetry axis of the Penning trap. Apertures in the sides of the Penning trap pass the fluorescence to a system of mirrors and lenses that direct the fluorescence to a fiber-optic bundle and then to a photomultiplier. A 100 MHz digitizing oscilloscope (Tektronix, Wilsonville, OR) captures the photomultiplier output. Each reported fluorescence intensity measurement represents an average from 10 laser shots. Except where noted, we carried out quadrupolar axialization by frequency sweep (chirp) excitation from 320 to 360 kHz with an amplitude of 10.8 V_{p-p} and a sweep rate of 10 Hz/μs in the presence of helium at a pressure of 1×10^{-5} torr. Axialization of the Ba^+ ions was extended for up to several minutes by repeating the above chirp excitations, spaced 0.002 s apart. We measured fluorescence intensity as a function of time by executing a series of measurements after each of a series of evolution periods (see below). A modular ICR data station (MIDAS [27]) served to control the experimental event sequence and detect ions by ion cyclotron resonance. The error bars in each figure represent the standard deviation for each data point.

Effects of Trapping Potential and Quadrupolar Axialization

We used LIF to determine the relative number of ions confined at different electrostatic trapping potentials. Ions formed during the ionization event were trapped by a combination of (relatively) high trapping potential and a background helium pressure of 1×10^{-5} torr. For 2.4 s following the ionization/trapping event, ions either expand radially or (under the influence of azimuthal quadrupolar excitation and buffer gas collisions) relax to the center of the trap. After that period, we measure the fluorescence intensity (five measurements at each trapping potential).

We measured the time evolution of fluorescence intensity (four intensity measurements at each time point) of trapped Ba^+ ions as a function of trapping potential (20, 100, and 280 V) in the presence and absence of quadrupolar axialization. Each group of experiments measured the time evolution of the fluorescence intensity of trapped Ba^+ ions at three different trapping potentials: 20, 100, and 280 V.

Effect of Pressure on Ion Fluorescence Intensity

We examined the effects of pressure on our fluorescence signal by measuring two fluorescence time courses. The time course of ion fluorescence was first observed at a fixed pressure of 6×10^{-6} torr by admitting gas into the vacuum chamber via a leak valve. Alternatively, the initial pressure was raised to 6×10^{-6} torr by a pulse of gas (from a pulsed valve) but was then allowed to drop steadily by pumping. By initiating each experiment at the same pressure, we hoped to minimize differences in ion number and ion cloud shape.

Effect of the Excitation Waveform on the Efficacy of Quadrupolar Axialization

We then measured the time course of fluorescence intensity for trapped ions in the presence of quadrupolar axialization, for three different excitation waveforms. All three excitation waveforms were frequency-sweep excitations with the same parameters as for all other quadrupolar axialization presented in this paper except for the range of frequencies swept. The first frequency sweep from 320 to 360 kHz was "resonant" with the barium ICR frequency of 340 kHz. We denote a second frequency sweep from 320 to 360 kHz as "below-resonance" excitation, and a third frequency sweep from 356 to 640 kHz as "above-resonance" excitation. We also measured a fluorescence time course under identical conditions without any quadrupolar axialization for comparison. We took four measurements at each time point.

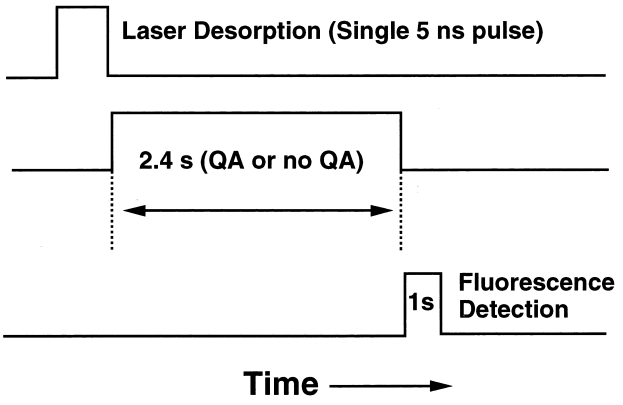

Figure 1. Experimental event sequence for determination of ion fluorescence intensity as a function of trapping potential.

Results and Discussion

With one exception, the results of the experiments described below conform well with our current understanding of FT-ICR theory and experiment. The anomalous result involves the choice of excitation waveform for azimuthal quadrupolar axialization, a topic which is itself not yet well understood (see below).

Effect of Trapping Potential on Ion Trapping Efficiency

Successful confinement of atomic Ba^+ ions required a trapping potential of 30–300 V applied to each endcap electrode of a three-section open cylindrical Penning trap. We measured the fluorescence induced from Ba^+ ions generated by laser desorption at different trapping potentials, following a 2.4 s evolution period (Figure 1) after the ionization event. In the *presence* of quadrupolar axialization during the evolution period (Figure 2, solid line), the Ba^+ fluorescence signal remained approximately constant over a trapping potential range of 70–280 V. [Over the same range of trapping potential, fewer ions remain near the trap symmetry axis in the *absence* of quadrupolar axialization (Figure 2, dotted line), as expected [26]]. At higher trapping potential, the fluorescence signal decreased sharply because of rapid expansion of ion magnetron radii during the 2.4-s interval between ion formation and LIF detection.

It is interesting to note that Beu et al. [28] observed a trapping potential dependence of laser-desorbed metal ions similar to that in Figure 2 when they placed a high retarding potential on the end cap of their Penning trap nearest the site of desorption. They attributed that behavior to a "Debye shielding" effect. The abrupt drop in number of fluorescence-detected ions at >300 V trapping potential is thus likely because of a breakdown in Debye shielding so that ions are no longer able to penetrate the trapping potential barrier to enter the trap.

Figure 3 illustrates the time dependence of the on-axis ion population (as reflected by ion fluorescence

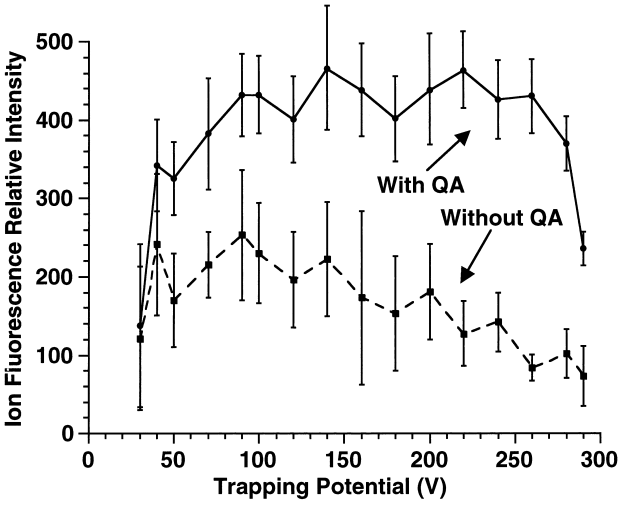

Figure 2. Ba^+ fluorescence intensity as a function of trapping potential, in the presence or absence of quadrupolar axialization during a 2.4-s interval between ion formation and ion fluorescence detection, as shown in the experimental event sequence of Figure 1. Note the pronounced drop in fluorescence signal with increasing trapping voltage, in the absence of quadrupolar axialization.

relative intensity), in the absence of quadrupolar axialization. Note that a larger trapping potential results in a larger initial fluorescence signal; thus, more ions are trapped on-axis initially. However, the rate of ion loss increases monotonically with increasing trapping potential, because of magnetron radial expansion from ion–neutral collisions. The situation is reversed in the presence of quadrupolar axialization (Figure 4): both the initial fluorescence signal and its duration increase with increasing trapping potential, because azimuthal quadrupolar excitation in the presence of buffer gas

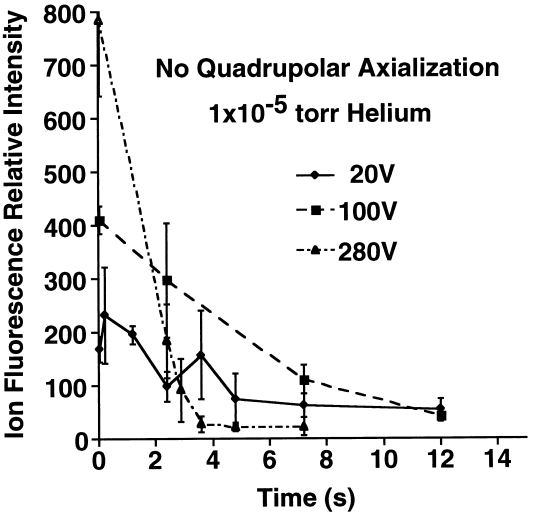

Figure 3. Ba^+ fluorescence intensity as a function of the period between ion formation and fluorescence detection, in the absence of quadrupolar axialization, at each of several trapping potentials. The experimental event sequence is otherwise like that of Figure 1, except that the fixed 2.4-s interval varies from 0 to 20 s.

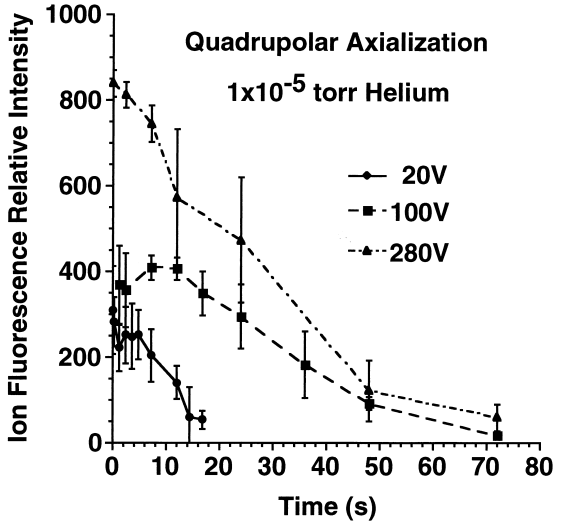

Figure 4. Ba^+ fluorescence intensity as a function of the period between ion formation and fluorescence detection, in the presence of quadrupolar axialization, at each of several trapping potentials. The experimental event sequence is otherwise like that of Figure 1, except that the fixed 2.4-s interval varies from 0 to 80 s. Both the initial fluorescence signal and its duration increase with increasing trapping potential when quadrupolar axialization is used.

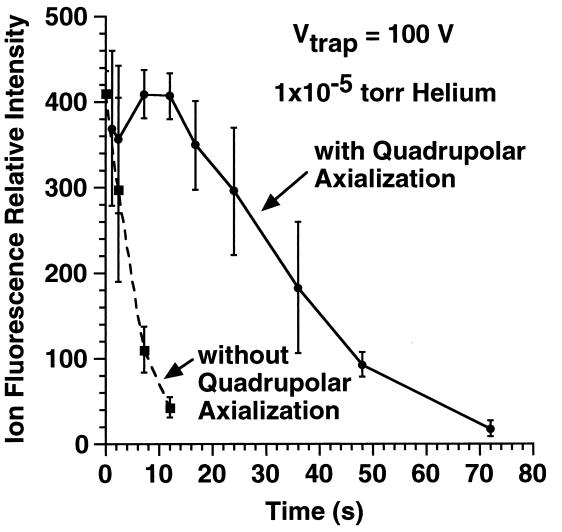

Figure 5. Ba^+ fluorescence intensity as a function of the period between ion formation and fluorescence detection, in the presence or absence of quadrupolar axialization, at 100 V trapping potential. Note the dramatic improvement in the duration of ion trapping in the presence of quadrupolar axialization.

collisions forces ions back to the trap axis, thereby greatly reducing outward radial diffusion. The effect is dramatic: the fluorescence (and thus relative number of on-axis ions) at a trapping potential of 280 V is initially ~3 times larger than that at a trapping potential of 20 V. In addition, the fluorescence persists for ~75 s at 280 V, but only for ~15 s at 20 V.

Effect of Quadrupolar Axialization

Figure 5 vividly demonstrates the efficacy of quadrupolar axialization. Ions are trapped for about five times longer with axialization than without it. The combined results of Figures 2–4 provide a particularly direct demonstration that quadrupolar axialization succeeds in increasing the length of time that ions can be confined in a Penning trap.

Pressure Effects on Ion Trapping Duration

We investigated the effects of pressure on the trapping duration of Ba^+ ions by measuring ion fluorescence intensity as a function of time under two different sets of conditions: a constant background pressure of 6×10^{-6} torr; or gas pulsed into the chamber at an initial pressure of 6×10^{-6} torr and pumped out during ion fluorescence detection (Figure 6).

The effect of pressure on trapping duration may then be seen from Figure 7. On removal of azimuthal quadrupolar excitation, at a constant pressure of 6×10^{-6} torr, the fluorescence signal decays to ~10% of its initial value after ~8 s. If, instead, a gas pulse to approximately the same initial pressure of $\sim 6 \times 10^{-6}$ torr is followed by immediate pumpdown, ~15% of the initial fluorescence intensity persists for ~25 s. Clearly, the diminishing pressure during the second experiment results in a longer trapping duration, because of fewer ion–neutral collisions and thus slower magnetron radial expansion [5, 29].

Resonant Versus Off-Resonant Quadrupolar Axialization

The effect of the choice of frequency-sweep (chirp) waveform for azimuthal quadrupolar excitation on the ion fluorescence signal is seen in Figure 8. Resonant excitation (i.e., chirp excitation spanning a frequency

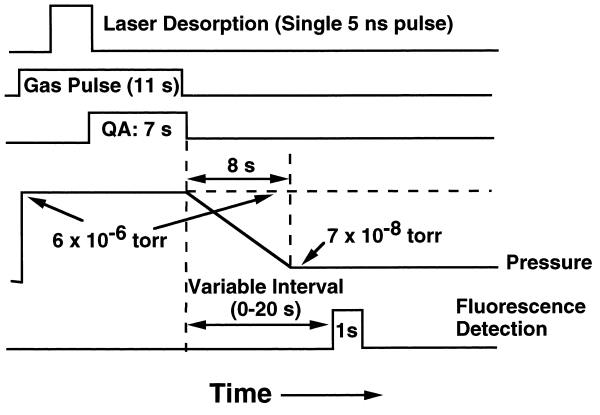

Figure 6. Experimental event sequence for determination of ion fluorescence intensity as a function of background gas pressure. Pressure is either held constant at 6×10^{-6} torr or initially pulsed at that pressure for 11 s and allowed to drop by continuous pumping of gas during a 0–20 s period following ion formation and axialization (QA).

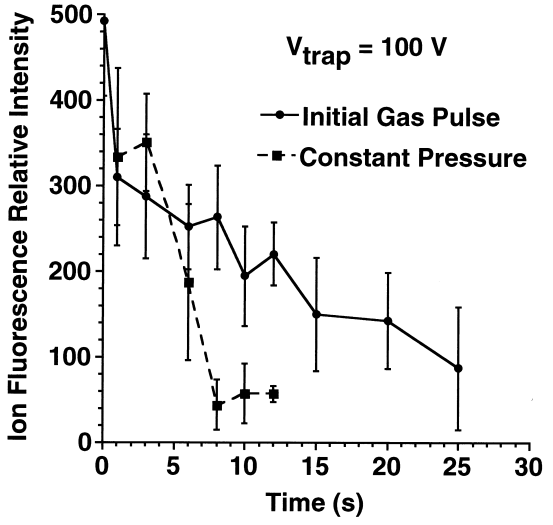

Figure 7. Ba^+ fluorescence intensity as a function of the variable interval (0–20 s) following ion formation and quadrupolar axialization, at 100 V trapping potential, for each of the two pressure regimes described in the event sequence of Figure 6. This comparison illustrates faster radial diffusion of ions at higher (constant) pressure than at lower (pulsed) pressure.

range including the reduced ion cyclotron frequency) and excitation by a chirp spanning frequencies below the reduced ion cyclotron frequency were comparably effective in axializing Ba^+ ions, whereas excitation with a chirp spanning frequencies above the reduced ion cyclotron frequency was far less effective. Nevertheless, even quadrupolar chirp excitation at frequencies above the reduced ion cyclotron frequency significantly improved the trapping during over an experiment performed in the absence of azimuthal quadrupolar excitation. We are currently investigating this peculiar frequency-response behavior.

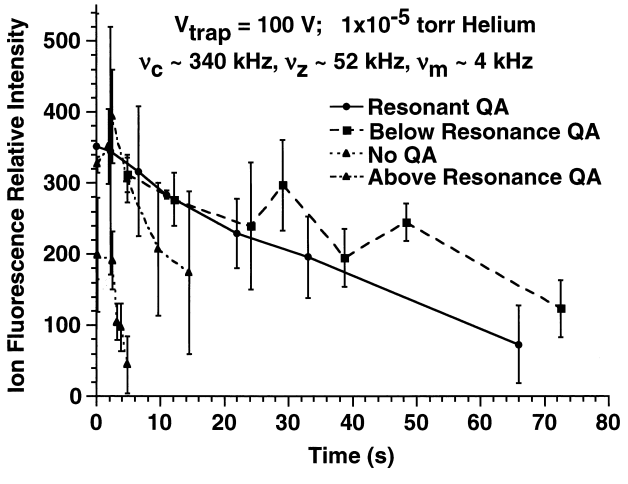

Figure 8. Ion fluorescence as a function of a period (0–100 s) of irradiation by resonant (320–360 kHz), below-resonance (36–320 kHz), and above-resonance (356–640 kHz) frequency-sweep excitation, for Ba^+ ions of unperturbed cyclotron frequency, 338 kHz. A control experiment with no quadrupolar excitation is also shown.

Axial Versus Radial Ejection

It is well known that increasing the trapping potential in an FT-ICR experiment decreases the length of time that ions remain trapped [30, 31]. Our fluorescence results confirm the mechanism underlying that observation. Figure 3 shows that, in the absence of quadrupolar axialization, ions move off-axis faster at higher trapping potential. However, the opposite is true in the presence of quadrupolar axialization (Figure 4): ions remain on-axis longer at higher trapping potential. Finally, Figure 7 shows that ions move off-axis faster (and the fluorescence detected from on-axis ions therefore decreases faster) at higher pressure. Taken together, those experiments confirm that (at 10^{-5} torr, for $\geq$20 V trapping potential), ions are lost more rapidly radially than axially, unless quadrupolar axialization is used.

Conclusions

LIF represents a new and useful probe for the analysis of ion dynamics in an FT-ICR experiment. Here, we have demonstrated its value for characterizing processes such as radially outward collisional ion cloud expansion and radially inward ion cloud compression, as well as the effects of trapping potential and pressure on those processes. The main advantage of this technique is that the fluorescence signal is directly related to the number of ions in the laser beam path. (Some loss in fluorescence intensity will occur if the ion cloud elongates along the z axis because our fluorescence detection efficiency is greatest near the middle of the trap. However, the high trapping voltages used in these experiments should severely limit ion expansion in the z direction. Therefore, we do not expect the lower fluorescence detection efficiency at the ends of the trap to be a problem.) The measurement therefore reports the relative number of ions in a comparatively small, localized region of the Penning trap. The present results confirm that, in the absence of quadrupolar axialization, magnetron expansion is the primary means of ion loss during a typical FT-ICR experiment. We also confirm that quadrupolar axialization increases the maximum duration of ion trapping by significantly reducing the rate of magnetron expansion. The efficacy of quadrupolar axialization is dramatically affected by the choice of excitation waveform, a result that deserves in-depth future scrutiny.

LIF ion tomography should prove useful for various future investigations of ion dynamics in a Penning trap. For example, it should be possible to map the one-, two-, and/or three-dimensional spatial distribution of an ion cloud under a variety of steady-state conditions by translating the position of the laser beam with respect to the ion trap. The technique could also be used

to monitor the response of an ion cloud to various dipolar and quadrupolar excitation schemes, various ion trap geometric and trapping potential configurations, as well as various modulations of end cap ("trapping") potential during an experimental event sequence. The effect of different buffer gases could be explored, along with the mechanism (Langevin versus hard sphere) for ion–neutral collisions [32]. Such extensions promise to provide many new insights into the shape and time behavior of an ion cloud in an FT-ICR mass spectrometer.

Acknowledgments

The authors thank S. Guan for numerous helpful conversations, suggestions, and insights. We thank C. L. Hendrickson for critical review of the manuscript. Work supported by the National Science Foundation (CHE-93-22824), Florida State University, and the National High Magnetic Field Laboratory in Tallahassee, FL.

References

1. Hunter, R. L.; Sherman, M. G.; McIver, R. T., Jr. *Int. J. Mass Spectrom. Ion Phys.* **1983,** *50*, 259–274.
2. Comisarow, M. B. *J. Chem. Phys.* **1978,** *69*, 4097–4104.
3. Limbach, P. A.; Grosshans, P. B.; Marshall, A. G. *Anal. Chem.* **1993,** *65*, 135–140.
4. Kerley, E. L.; Russell, D. H. *Anal. Chem.* **1989,** *61*, 53–57.
5. Guan, S.; Huang, Y.; Xin, T.; Marshall, A. G. *Rapid Commun. Mass Spectrom.* **1996,** *10*, 1855–1859.
6. Drullinger, R. E.; Wineland, D. J.; Bergquist, J. C. *Appl. Phys.* **1980,** *22*, 365–368.
7. Thompson, R. C.; Barwood, G. P.; Gill, P. *Appl. Phys. B* **1988,** *46*, 87–93.
8. Bollinger, J. J.; Wells, J. S.; Wineland, D. J.; Itano, W. M. *Phys. Rev. A* **1985,** *31*, 2711–2714.
9. Itano, W. M.; Bergquist, J. C.; Wineland, D. J. *J. Opt. Soc. Am. B* **1985,** *2*, 1392–1394.
10. Hubrich, M.; Knab, H.; Knoll, K. H.; Werth, G. *Z. Phys. D* **1991,** *18*, 113–115.
11. Knab, H.; Knoll, K. H.; Scheerer, F.; Werth, G. *Z. Phys. D* **1993,** *25*, 205–208.
12. Wineland, D. J.; Itano, W. M.; Van Dyck, R. S. J. *Adv. At. Mol. Phys.* **1983,** *19*, 135–186.
13. Dehmelt, H. *Rev. Mod. Phys.* **1990,** *62*, 525–530.
14. Blatt, R.; Gill, P.; Thompson, R. C. *J. Mod. Opt.* **1992,** *39*, 193–220.
15. Werth, G. *Phys. Scri.* **1995,** *T59*, 206–210.
16. Mahan, B. H.; Martner, C.; O'Keefe, A. *J. Chem. Phys.* **1982,** *76*, 4433–4438.
17. Kato, S.; Frost, M. J.; Bierbaum, V. M.; Leone, S. R. *Rev. Sci. Instrum.* **1993,** *64*, 2808–2820.
18. Welling, M.; Schuessler, H. A.; Thompson, R. I.; Walther, H. *Int. J. Mass Spectrom. Ion Processes* **1998,** *172*, 95–114.
19. Hemberger, P. H.; Nogar, N. S.; Williams, J. D.; Cooks, R. G.; Syka, J. E. P. *Chem. Phys. Lett.* **1992,** *191*, 405–410.
20. Williams, J. D.; Cooks, R. G.; Syka, J. E. P.; Hemberger, P. H.; Nogar, N. S. *J. Am. Soc. Mass Spectrom.* **1993,** *4*, 792–797.
21. Cleven, C. D.; G., C. R.; Garrett, A. W.; Nogar, N. S.; Hemberger, P. H. *J. Phys. Chem.* **1996,** *100*, 40–46.
22. Alheit, R.; Gudjons, T.; Kleinedam, S.; Werth, G. *Rapid Commun. Mass Spectrom.* **1996,** *10*, 583–590.
23. Li, G.-Z.; Vining, B. A.; Guan, S.; Marshall, A. G. *Rapid Commun. Mass Spectrom.* **1996,** *10*, 1850–1854.
24. Guan, S.; Marshall, A. G. *Rapid Commun. Mass Spectrom.* **1993,** *7*, 857–860.
25. Guan, S.; Wahl, M. C.; Marshall, A. G. *J. Chem. Phys.* **1994,** *100*, 6137–6140.
26. Guan, S.; Kim, H. S.; Marshall, A. G.; Wahl, M. C.; Wood, T. D.; Xiang, X. *Chem. Rev.* **1994,** *94*, 2161–2182.
27. Senko, M. W.; Canterbury, J. D.; Guan, S.; Marshall, A. G. *Rapid Commun. Mass Spectrom.* **1996,** *10*, 1839–1844.
28. Beu, S. C.; Hendrickson, C. L.; Vartanian, V. H.; Laude, D. A., Jr. *Int. J. Mass Spectrom. Ion Processes* **1992,** *113*, 59–79.
29. Francl, T. J.; Fukuda, E. K.; McIver, R. T., Jr. *Int. J. Mass Spectrom. Ion Processes* **1983,** *50*, 151–167.
30. Hendrickson, C. L.; Hofstadler, S. A.; Beu, S. C.; Laude, D. A., Jr. *Int. J. Mass Spectrom. Ion Processes* **1993,** *123*, 49–58.
31. Beu, S. C.; Laude, D. A., Jr. *Int. J. Mass Spectrom. Ion Processes* **1991,** *108*, 255–268.
32. Guan, S.; Li, G.-Z.; Marshall, A. G. *Int. J. Mass Spectrom. Ion Processes* **1998,** *167/168*, 185–194.